The origin of hierarchical cracks in floor-fractured craters on Mars and the Moon

Axel Montigny, Damian Walwer, Chloé Michaut

Earth and Planetary Science Letters 600 (2022) 117887

Contents lists available at ScienceDirect

Earth and Planetary Science Letters

journal homepage: www.elsevier.com/locate/epsl

The origin of hierarchical cracks in floor-fractured craters on Mars and the Moon

Axel Montigny [a], Damian Walwer [a,1], Chloé Michaut [a,b,*]

[a] Ecole Normale Supérieure de Lyon, Université Claude Bernard Lyon 1, Université de Lyon, UJM, CNRS, Laboratoire de Géologie de Lyon, Terre, Planètes, Environnement, 69007 Lyon, France
[b] Institut Universitaire de France, France

ARTICLE INFO

Article history:
Received 8 April 2022
Received in revised form 21 October 2022
Accepted 21 October 2022
Available online 3 November 2022
Editor: W.B. McKinnon

Keywords:
floor-fractured craters
hierarchical cracks
magmatic intrusion
desiccation
Mars
the Moon

ABSTRACT

Numerous craters showing floor fractures have been identified on the Moon and Mars. Whereas on the Moon, the floor morphology, crater geology and fracture characteristics suggest that the floor deformation is caused by underlying magmatic intrusions, the origin of fractures and floor modifications of Martian floor-fractured craters (FFCs) remains debated. Here, we focus on FFCs displaying hierarchical crack patterns. We use different quantitative fracture characteristics to investigate the physical processes at the origin of cracks and compare their variations to scaling laws derived theoretically and from desiccating laboratory experiments. We show that cracks on a large set of Martian FFCs close to Valles Marineris differ from that of Lunar FFCs: they may be explained by tensile stresses caused by the shrinkage of a material adhering on the crater floor, similar to desiccating cracks. Other Martian FFCs close to Syrtis Major show cracks more similar to those caused by a magmatic intrusion.

1. Introduction

Floor-fractured craters (FFCs) are peculiar impact craters that present fractured and uplifted floors. They are distinguishable from regular impact craters that do not display signs of morphological modifications. FFCs were initially identified on the Moon but are now also observed on Mars, Venus and Ceres (Schultz, 1976; Wichman and Schultz, 1995; Bamberg et al., 2014; Buczkowski et al., 2018). While two mechanisms were originally proposed to explain the cause of floor deformation and fracturing of Lunar FFCs: (1) intrusion of magma in the subsurface below the craters (Schultz, 1976) or (2) viscous relaxation of the crater floor (Hall et al., 1981), the magmatic intrusion hypothesis appears to be more consistent with observations. Lunar FFCs floor topography, the presence of intra-crater vents and associated signs of magmatic extrusion as well as FFCs gravity anomaly signature all seem to testify of the presence of an underlying magmatic intrusion (Gaddis et al., 2003; Jozwiak et al., 2012; Thorey and Michaut, 2014; Thorey et al., 2015).

Several mechanical models have been proposed to explain magma ascent and shallow emplacement despite its negative buoyancy within the Lunar crust (Wilson and Head, 2017; Head and Wilson, 2017). For example, comparing observations and evidence of magma intrusions and extrusions on mare-filled and floor-fractured Lunar craters with mechanical models of vertical dyke propagation, Michaut and Pinel (2018) proposed that the unloading caused by the mass deficit associated to the crater can drive magma ascent in the low-density Lunar crust. This driving mechanism seems also consistent with the observed total fracture length at FFC floors, a quantity that can be used to constrain mechanical models of fracture formation (Ghabache et al., 2016) and in particular crater-centred intrusion processes in the Lunar crust (Walwer et al., 2021).

On Mars, various causes have been proposed to explain crater floor modifications and subsequent fracturing, including deformation of magmatic, hydraulic, glacial or tectonic origin (Bamberg et al., 2014; Sato et al., 2010; Luzzi et al., 2021). Volcano-ice interaction has also been proposed to explain the chaotic aspect of some FFCs floors (Schultz, 1978; Korteniemi et al., 2006). Although the morphology of Martian FFCs appear in some cases similar to that on the Moon, Korteniemi et al. (2006) noted that some Martian FFCs may have wider and more numerous fractures than their Lunar counterpart.

Hierarchical crack patterns can be recognized on FFCs floors both on Mars and the Moon. Such a pattern refers to fractures

* Corresponding author at: Ecole Normale Supérieure de Lyon, Université de Lyon, UCBL, UJM, CNRS, Laboratoire de Géologie de Lyon, Terre, Planètes, Environnement, 69007 Lyon, France.
E-mail address: chloe.michaut@ens-lyon.fr (C. Michaut).
[1] Now at Department of Geosciences, Pennsylvania State University, University Park, PA, USA.

https://doi.org/10.1016/j.epsl.2022.117887

that are orthogonal to each other; they are said to be hierarchical because their formation follows both a temporal and spatial hierarchy. When a fracture first divides a medium, tensile stress is released in the direction perpendicular to it in such a way that the following fracture is perpendicular to previous ones (Bohn et al., 2014a). Because FFCs on the Moon are considered as resulting from emplacement of magmatic intrusions below impact craters, floor fractures in general and hierarchical crack patterns in particular, are assumed to form from stress build up within the subsurface induced by floor uplift and deformation (Thorey and Michaut, 2014; Walwer et al., 2021). Recent analog experiments have shown that inflation or deflation produced by the injection of fluid into a deforming medium mimicking magma intrusion emplacement indeed causes fracture patterns similar to the one observed at FFCs (Poppe et al., 2019; Luzzi et al., 2021).

The presence of hierarchical crack patterns on the floor of FFCs on the Moon and Mars could suggest that magma intrusions below craters can occur on both planetary bodies. However, hierarchical fractures can also form in desiccating or cooling material (Ghabache et al., 2016; Bohn et al., 2014a,b; Dufresne et al., 2003; Bahr et al., 2010; Gauthier et al., 2010; Flores, 2017; Cho and Datta, 2019; Ma et al., 2019). The homogeneous volumetric contraction occurring during these processes is limited by adhesion onto a rigid substrate that induces tensile stress accumulation in the shrinking material. Cracks start to appear when the stress in the deformed volume reaches a critical value. During fracturing, stresses perpendicular to the fractures are released while stresses parallel to it subsist. Thus, a newly formed crack joins the previous one perpendicularly to it. A fracture network appears in this way, delineating several domains. Many studies on the desiccation of thin films of hydrated material have shown that the characteristic size of these domains, or distance between cracks, increases with the layer thickness (Dufresne et al., 2003; Bohn et al., 2014a,b; Cho and Datta, 2019; Flores, 2017; Ma et al., 2019).

Here, we analyse quantitatively the crack characteristics of Martian and Lunar craters presenting a hierarchical crack pattern in order to provide insights into the mode of deformation and stress build up in the material forming the floor of FFCs. In particular, we aim at understanding whether the hierarchical fracture pattern of Martian and Lunar FFCs results from the same mechanism. To do so, we measure the total fracture length and estimate the characteristic size of the domains delimited by cracks. Guided by the results of the drying experiments we performed as well as by theoretical relationships derived from Griffith's theory of brittle fracture, we test whether the observed fracture characteristics are more likely due to magma intrusion processes or to tensile stresses caused by the contraction of crater-filling material adhering on the floor.

2. Floor-fractured craters and desiccating experiments

2.1. Hierarchical fracture patterns

Hierarchical fracture patterns can be seen as a form of self-organized crack patterns (Gauthier et al., 2010). It corresponds to fractures that are orthogonal to each other and that divides a surface in several domains. Examples of hierarchical fracture patterns covering FFCs floors on the Moon and Mars as well as resulting from drying experiments are displayed in Fig. 1A-D.

The term hierarchical refers to both the temporal and spatial hierarchy of the fracture system (Bohn et al., 2014a). The temporal hierarchy is due to the time sequence of fracture formation: when a fracture first divides a medium in two domains, stress is released perpendicularly to it in such a way that, if a new fracture is formed afterward, it appears perpendicular to the previous one and divides the previously formed domain into two. The spatial hierarchy refers to the different domains that are delimited by the fractures: the material is first divided into two large domains that are themselves divided into smaller domains as more fractures break the deforming volume.

The temporal and spatial hierarchy result from both the history of stress build up and the spatial distribution of the stress field in the deforming volume (Bohn et al., 2014a; Tang et al., 2006; Cohen et al., 2009; Ghabache et al., 2016). Recognizing the occurrences of hierarchical fracture patterns on the floor of Lunar and Martian FFCs can therefore provide insights into the process of stress build up and deformation at those craters in a new and original way.

2.2. FFCs displaying hierarchical cracks

2.2.1. Data sets and crater selection

Fracture patterns on crater floors can be inspected visually using night and day THEMIS (Thermal Emission Imaging System) images available for Mars and LROC (Lunar Reconnaissance Orbiter Camera) images for the Moon. Both data sets have a resolution of 100 meters per pixels. We also used MOLA and LOLA digital elevation models (DEMs) with a resolution of 128 pixels per degree for both the Moon and Mars. All mentioned data-sets are freely available at the NASA Geosciences Node archives (https://pds-geosciences.wustl.edu/dataserv/). We selected craters whose floors were clearly fractured with well-visible cracks orthogonal to each other, i.e. showing T-junctions, and delimiting several domains on the crater floor. Craters with fissures extending beyond the crater floors were excluded from our analysis. Craters displaying a hierarchical crack pattern are shown in Fig. 1C,D along with FFCs displaying a different fracture pattern (Fig. 1E,F). Other examples of both types are given in Supplementary Figures S1 to S11.

Going through the 383 Martian craters qualified as fractured in the database of Robbins and Hynek (2012), we found that 25 satisfy our criteria. Most selected craters are located East of Valles Marineris and West of Arabia Terra, within Xanthe Terra and Margaritifer Terra and six of them around the Isidis Basin, close to Syrtis Major or to Amenthes Planum (Bottom of Fig. 2). On the Moon, among the 155 craters belonging to the Lunar FFCs database of Jozwiak et al. (2012), 19 present a hierarchical fracture pattern and appear to be more evenly distributed on the Lunar surface compared to Martian ones (Top of Fig. 2).

2.2.2. Estimating floor uplift or crater infilling thickness

A key quantity exploited here and characterising FFCs is the difference between an empirically inferred depth d^{th} and the observed FFC depth d^{obs},

$$\Delta d = d^{th} - d^{obs}. \tag{1}$$

The depth d^{th} depends only on the crater diameter D and constitutes an estimation of the crater depth –defined as the distance between crater rim and floor– before it has undergone modifications. We used the following relationships:

$$d^{th} = 0.315 D^{0.520}, \tag{2}$$

$$d^{th} = 1.044 D^{0.301}, \tag{3}$$

for Mars (2) and the Moon (3) respectively, where d^{th} and D are expressed in kilometre. The relation (2) was obtained empirically from all Martian fresh complex craters ($D \geq 7$ km) (Boyce and Garbeil, 2007). Similarly, the relation (3) was obtained from all Lunar fresh complex craters (Pike, 1977). Other relations linking crater size and depth, determined by Robbins and Hynek (2012) for example, were also tested with no significant changes in the results. The observed depth d^{obs} was obtained directly from the Moon and

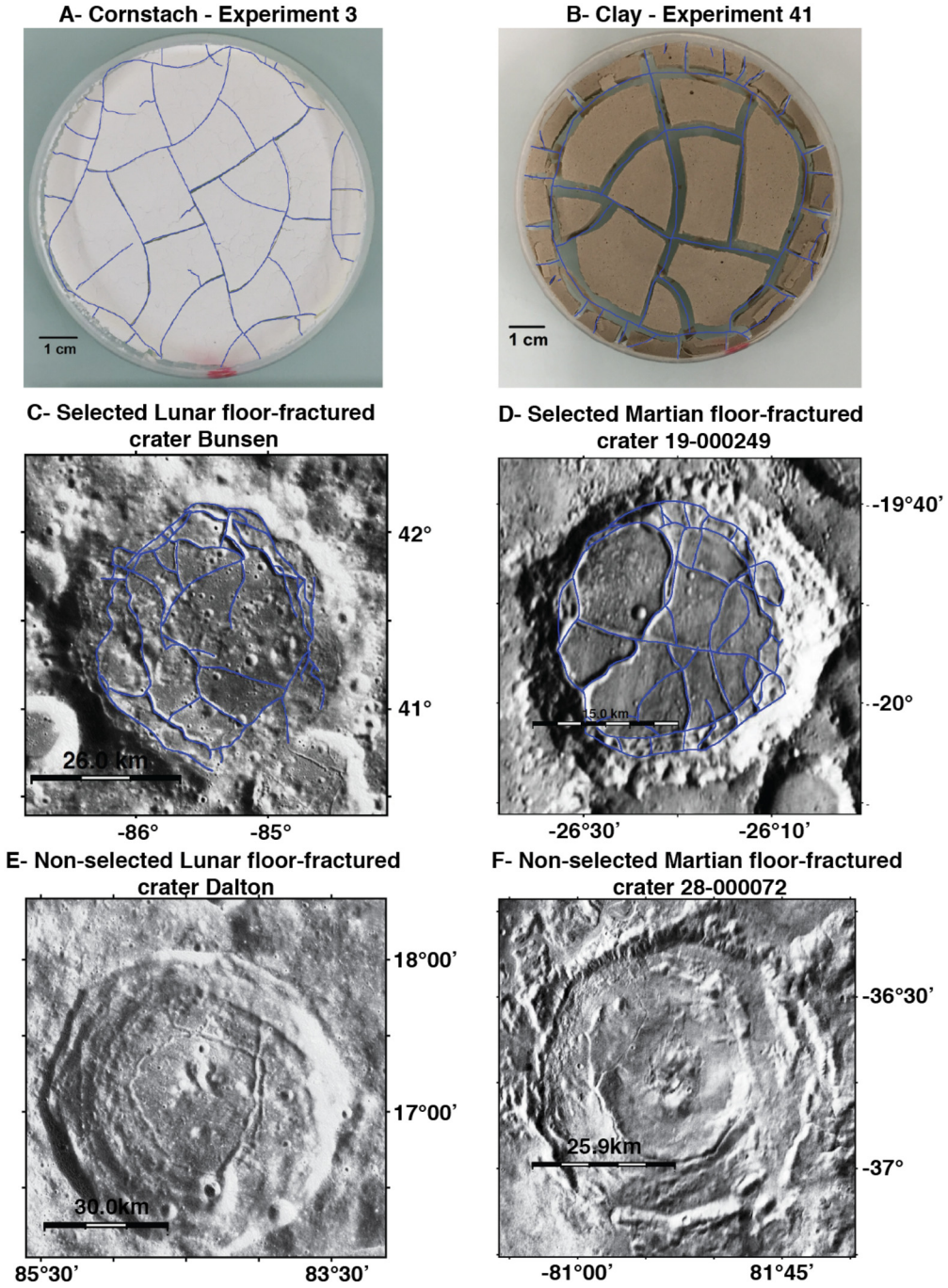

Fig. 1. Examples of fracture patterns from drying experiments as well as Martian and Lunar FFCs. Top and Middle panels: Hierarchical crack patterns associated to A), cornstach drying experiment 3, B) surfine green clay drying experiment 41, C) Lunar FFC Bunsen and D) Martian FFC 19-000249. Bottom panels: examples of FFCs that were not selected for this study because they do not present a hierarchical fracture pattern on their floors, E) Lunar FFC Dalton, F) Martian FFC 28-000072. Both display a circular fracture pattern. For A) to D) the mapping of fractures is shown in blue. (For interpretation of the colours in the figure(s), the reader is referred to the web version of this article.)

Mars DEMs by calculating the rim-to-floor depth using topographic profiles centred on the selected crater. The final value used for d^{obs} constitutes an average corresponding to four different profiles with azimuths of 0° N, 45° N, 90° N and −45° N. The depth uncertainties are simply the standard deviations of the depth extracted from the four profiles at each crater.

The quantity Δd is interpreted in two different ways in this study. If the FFC results from deformation caused by an underlying magmatic intrusion, Δd constitutes an estimate of crater floor uplift (Wichman and Schultz, 1996; Walwer et al., 2021; Jozwiak et al., 2012). In the case where the FFC is filled with exogenous material, Δd provides an estimate of the filling thickness.

2.3. Drying experiments

To gain insight into the mode of deformation that may lead to the formation of a hierarchical fracture pattern on the Moon and Mars, we performed desiccating experiments. Although the exact mechanism leading to fracture formation in those experiments may be different from the one associated to FFCs, they allow to investigate whether a scenario where a cylindrical volume contracts

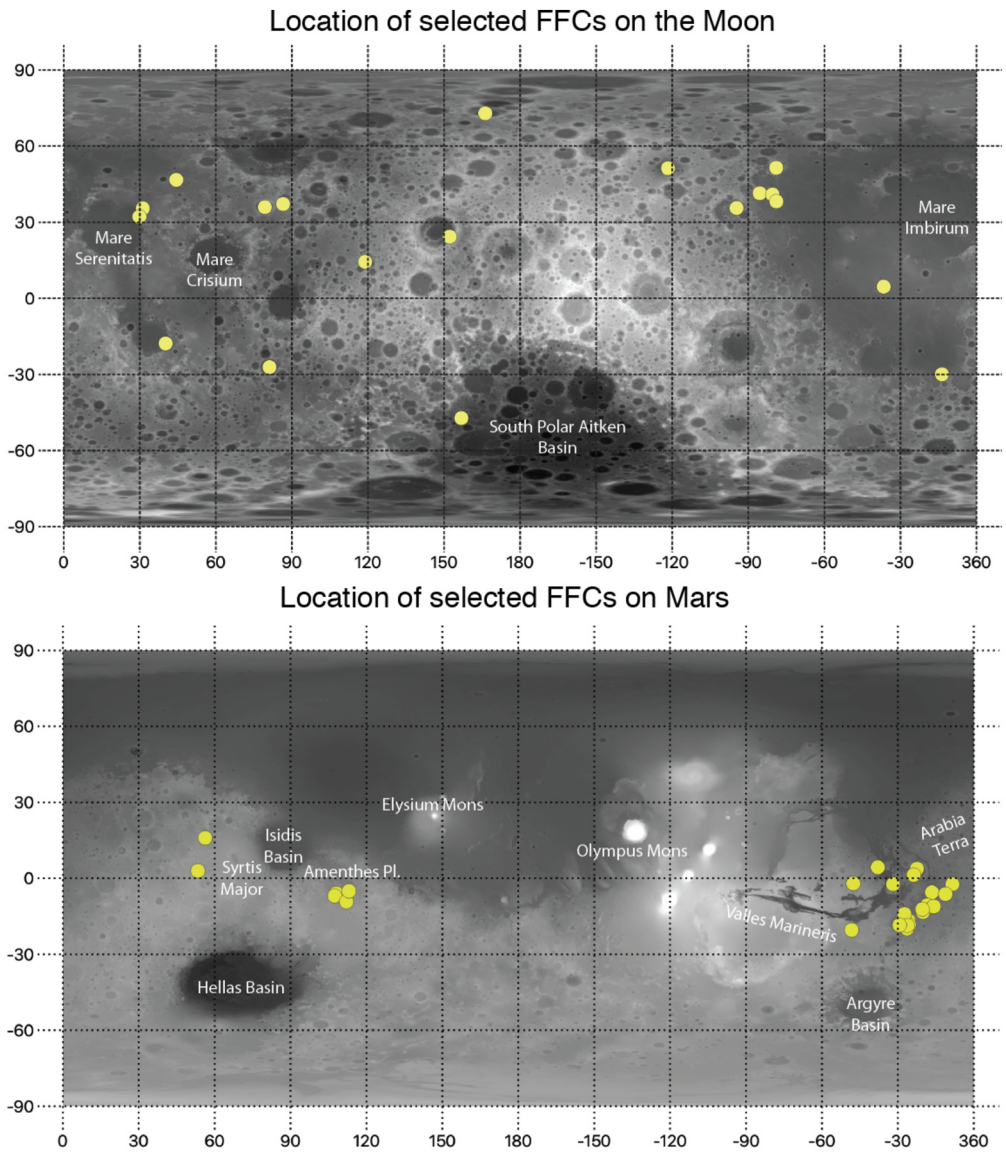

Fig. 2. Location of floor-fractured craters presenting cracks with a hierarchical pattern on the topographic background of the Moon (top) and Mars (bottom).

while adhering on a substrate can eventually explain the observed FFCs morphological features.

For our desiccating experiments, we use a solution of cornstarch from MAÏZENA and water with a ratio of 1 to 1.14 g respectively (Bohn et al., 2014b). We also use a solution of Montmorillonite surfine green clay from LAINO and water with a ratio of 1 to 1.30 g. These ratios were chosen for the solution to be homogeneous and fluid enough to distribute easily within the different containers. Different circular containers are filled with our two types of mixtures made homogeneous upon mixing: plastic petri dishes (Diameter Ø= 8,7 cm) and glass crystallizers (Ø= 5.6; 8.8; 9.1; 9.7; 13.5; 18.5; 18.7 cm). Experiments are placed under temperature-controlled conditions, at 50 °C (323 K). Humidity is not controlled. Other experiments, run under different temperature conditions, show similar total crack length and number of domains. More than 80 experiments were realised with different thicknesses. Such types of experiments were already analysed similarly in many previous studies (Bohn et al., 2014b). Unlike in previous studies, we vary not only the layer thickness but also the container size. Once dry, we measure the final layer thickness h with a caliper with a precision of 10^{-3} cm.

The solutions typically take 5 to 10 hours to dry. Surfine green clay and water mixtures only show a hierarchical crack pattern upon drying (Fig. 1B). However, during desiccation of cornstarch and water mixtures (Fig. 1A), two successive types of cracks appear (Bohn et al., 2014a). Hierarchical cracks appear first; they directly affect the full layer thickness and appear one after the other. They propagate horizontally from their location of first occurrence. Smaller polygonal types of cracks appear in the late drying stage; they all appear at about the same time at the surface and propagate vertically from the surface down to the bottom. The mechanisms at the origin of these different types of fractures are different and have been described in previous studies (Ma et al., 2019). In this study, we focus our observations on the largest, primary, hierarchical cracks that appear in all experiments and that form altogether a closed network of hierarchical fractures delimiting adjacent domains of similar size (Fig. 1A,B).

2.4. Characterising the observed fracture systems

Quantitative characterisations of the fracture system were performed in the exact same way for FFCs and experiments. The choice of the measured quantities presented here is motivated by

the theoretical arguments developed in Section 3. For each crater and experiment, we measured the total fracture length L using the ImageJ software, as in Walwer et al. (2021), and counted the number of domains N delimited by fractures (Fig. 1 A and B). When a fracture does not completely separate a domain into 2, we counted 1.5 domains rather than 2. We estimated the area A of the crater floor affected by the fractures from that of the smallest disk encompassing all mapped fractures and whose centre corresponds to the crater centre. Except for one crater (19-000446 Supplementary Figure S5, which presents a zone devoid of fractures in its north-eastern part), the fractures extend over the full crater floors. For drying experiments, the area A is that of the container, also circular.

For both FFCs and experiments we estimated the characteristic size of domains delimited by fractures, or characteristic distance between cracks l. One definition of l, denoted l_1, which is generally used in studies on desiccation of hydrated material (Bohn et al., 2014a,b; Cho and Datta, 2019; Ma et al., 2019), is the square root of the initial area A of material affected by the cracks divided by the total number of domains N:

$$l_1 = \sqrt{\frac{A}{N}}. \tag{4}$$

We introduce a second way of estimating the characteristic domain size, denoted l_2, which depends on the total fracture length L:

$$l_2 = \frac{A}{L}. \tag{5}$$

Further details about the measurements and error estimates of each quantity mentioned above are provided in Section S1 of the Supplementary Material.

3. Theoretical relationships involving cracks characteristics

3.1. Griffith theory of brittle fracture

The formation of fractures in a brittle material corresponds to the creation of new interfaces. According to Griffith's theorem of brittle fracture, crack formation within a medium requires that the available bulk energy of deformation in a volume V becomes larger or equal to the energy needed to create new crack interfaces ΓS. The so called fracture or Griffith energy Γ is assumed to be a material constant and corresponds to an energy per unit surface; S is the newly formed surface (Griffith, 1921). The Griffith criterion for fracture formation can express

$$\frac{\bar{\sigma}^2}{2E} V \geq \Gamma S, \tag{6}$$

where $\bar{\sigma}$ is a mean value of the stress averaged over the volume (Ghabache et al., 2016; Landau et al., 1986; Flores, 2017; Ma et al., 2019). Scaling laws derived from this theory were successfully applied to various systems involving a wide range of fracture patterns (Ghabache et al., 2016; Cohen et al., 2009; Vermorel et al., 2010; Vandenberghe et al., 2013). Here we exploit such a framework to the various hierarchical fracture patterns we study. The aforementioned theory is used to express scaling laws relating parameters involved either in the magma intrusion process or in the volumetric contraction of a layer adhering on a substrate with the observed fracture characteristics presented in Section 2.4 (Ghabache et al., 2016; Walwer et al., 2021; Flores, 2017). The main assumption underlying this approach in the context of systems displaying hierarchical fracture patterns is that elasticity remains valid as the fracture system develops (Flores, 2017).

3.2. Cracks formed by an intrusion deforming and uplifting its roof

When magma intrudes below and uplift an elastic layer of thickness T over a wavelength Λ, it exerts an overpressure ΔP at the layer base. In that case, an average value for the stress, estimated from the volume-averaged stress tensor, scales with (Landau et al., 1986; Flores, 2017; Walwer et al., 2021)

$$\bar{\sigma} \propto \frac{\Delta P \Lambda}{T}. \tag{7}$$

Using this expression for $\bar{\sigma}$ in (6) and considering that the deformed volume V scales as $\Lambda^2 T$ and that the entire energy of deformation within the overburden is dissipated by the creation of new fractures we obtain:

$$\frac{\Delta P^2 \Lambda^4}{2ET} \propto \Gamma L T, \tag{8}$$

where L is the total fracture length and we assume that the fractures propagate through the whole elastic layer thickness T. Fractures form and propagate as the intrusion spreads laterally and uplifts the overburden; the quantity L should thus reflect the overpressure ΔP driving emplacement, while the characteristic domain size separating two fractures may vary as the intrusion progressively spreads and affects a wider area.

Assuming as in Walwer et al. (2021) that the development of fractures dissociates the intrusion roof from the surrounding crust, favouring further thickening of the intrusion, the driving pressure for the intrusion may be counterbalanced by its own weight, i.e.,

$$\Delta P = \rho_m g H, \tag{9}$$

where H is the intrusion thickness, ρ_m magma density and g gravitational acceleration (Pollard and Johnson, 1973; Wichman and Schultz, 1996; Jozwiak et al., 2012). Using Δd as an estimate of floor uplift and assuming that the uplift directly reflects the intrusion thickness H, we obtain the following relation between L and Δd (Walwer et al., 2021):

$$L \propto \frac{\Delta d^2}{2E\Gamma} \left(\frac{\rho_m g \Lambda^2}{T} \right)^2 \Leftrightarrow \Delta d \propto \frac{T}{\rho_m g \Lambda^2} \sqrt{2E\Gamma L}. \tag{10}$$

Accordingly, in the case of a magmatic intrusion and provided that most of the energy of elastic deformation is dissipated through the formation of fractures, the total fracture length L is proportional to the square of the intrusion thickness Δd. This scaling law also shows that L evolves with other quantities such as T and Λ. However, the wavelength of the deformed volume Λ is expected to increase with T, for instance with $T^{3/4}$ in the case of a thin elastic plate (Michaut, 2011), the effects of the variations of these two quantities may thus partially compensate for each other.

3.3. Cracks formed by contraction of a material adhering on its substrate

Experiments involving deformation induced by contraction can provide insights about the occurrence of hierarchical fracture patterns (Allain and Limat, 1995; Bohn et al., 2014a,b; Bahr et al., 2010; Gauthier et al., 2010). Regardless of the physical mechanism causing deformation, it corresponds to a situation where a given volume shrinks homogeneously over a fixed substrate in such a way that the bottom boundary of the deformed material does not slip. Numerous experiments in thin desiccating films, for example, have shown that, when a hierarchical pattern develops, the characteristic size l of the domains delimited by fractures increases with the layer thickness h according to the power law $l \propto h^{\alpha}$ with α

ranging from 1/2 to 1 (Allain and Limat, 1995; Bohn et al., 2014b; Flores, 2017).

Those empirically-inferred power laws can be explained by theoretical arguments based on Griffith's theory (Gauthier et al., 2010; Flores, 2017). Following Flores (2017) and Ma et al. (2019), we consider a cell of elastic material with initial volume $V_n \approx A_n h$ separated by fractures which keeps being submitted to contraction. Using the fact that the average stress in a volume element can be related to an integral over the forces acting on its boundaries, one can relate the volume-averaged tensile stress $\bar{\sigma}$ in the film to the tensile stress σ_T acting on the bottom of the volume V_n (Landau et al., 1986, p.6-7):

$$\bar{\sigma}^2 \propto \frac{\sigma_T^2 A_n}{h^2}. \tag{11}$$

From (11) and (6), breaking the cell by forming a new fracture interface of surface $\sqrt{A_n}h$ implies that

$$\frac{\sigma_T^2 A_n}{2h^2 E} A_n h \geq \Gamma \sqrt{A_n} h. \tag{12}$$

Assuming that the energy of deformation within the cell is entirely dissipated by the formation of fractures, we obtain that

$$A_n^{3/2} = \frac{2\Gamma E}{\sigma_T^2} h^2, \tag{13}$$

showing that the domain area of the isolated cell increases with the film thickness h to the power 4/3 with a coefficient of proportionality that depends on material mechanical properties E and Γ as well as on the tensile stress σ_T due to adhesion on the substrate. It results in a characteristic domain size $l \sim \sqrt{A_n}$ that increases with the layer thickness h as

$$l \propto h^{2/3}. \tag{14}$$

4. Results

4.1. Relationships between thickness h, fracture length L and domain size l for drying experiments

Our experiments show that both estimates of the characteristic domain size l_1 and l_2 increase with the layer thickness h (Fig. 3A and 3B) and we verify that this relationship does not depend on the container size. They confirm further the existence of a power-law relationship between the thickness h and the characteristic domain size l

$$l \propto h^{\alpha}, \tag{15}$$

shown in previous studies (Bohn et al., 2014a,b; Flores, 2017; Cho and Datta, 2019; Ma et al., 2019; Dufresne et al., 2003). For the experiments involving cornstarch, a linear regression accounting for error bars on our data points gives $\alpha = 0.70 \pm 0.02$ and $\alpha = 0.72 \pm 0.02$ for l_1 and l_2 respectively while for experiments involving clay, we find $\alpha = 0.51 \pm 0.03$ and $\alpha = 0.54 \pm 0.02$ respectively. The theoretical power-law relationship between the characteristic distance and the filling thickness with an exponent equal to 2/3 (Section 3.3) is consistent with our experimental results whether the characteristic domain size is defined by l_1 or l_2 (Fig. 3A and B). On the contrary no specific relation seems to exist between the total fracture length L and the thickness h for drying experiments (Fig. 4A).

4.2. Relationships between Δd, the total fracture length L and domain size l for FFCs

For Lunar FFCs, Δd increases with the total fracture length L (Fig. 4B). This trend was already observed by Walwer et al. (2021) for a larger set of FFCs not only including the ones displaying hierarchical crack patterns. The linear regression line that best fits the data points in Fig. 4B has a slope of 0.2 ± 0.2. On the contrary, the selected Martian FFCs do not follow such a trend between the total fracture length L and Δd (Fig. 4B).

For Mars, both l_1 and l_2 increase with Δd with a best-fit power-law exponent equal to 0.6 ± 0.1 for l_1 and 0.5 ± 0.2 for l_2 (Fig. 3C), which is between 0.5 and 1 and close to the theoretical value of 2/3 and to the ones inferred empirically from our experimental data points (Section 3.3 and Fig. 3 A,B). The data points for Lunar FFCs are, in comparison, much more scattered: they do not show a clear trend between l_1 or l_2 and Δd. The best-fit exponent is very different and is equal to 1.4 for both l_1 and l_2, and its estimated uncertainty is much larger (± 0.6 in both cases) reflecting the scattering of the data points.

In addition, apart from the 6 Martian FFCs with the largest value of $\Delta d \geq 1$ km, the trend followed by Martian data points is clearly distinct from the one followed by Lunar data points (Fig. 3). The values of Δd for the selected Martian craters range from one to several hundreds of meters and are in general smaller than Lunar FFCs values that are always larger than 1 km (Fig. 3C).

5. Discussion

5.1. Phenomenological insights from drying experiments

Our experimental results confirm that, for desiccation processes where the shrinkage of a material adhering onto its substrate generates hierarchical cracks, the characteristic size of the domains l delimited by fractures increases with the layer thickness h and follows a power-law $l \propto h^{\alpha}$ with $\alpha \sim 2/3$. It is consistent with the theoretical relationship presented in Section 3.3 and originally proposed by Flores (2017) and Ma et al. (2019). This result holds regardless of the type of drying material (Fig. 3). This is interesting because the morphology of individual cracks differs between the experiments involving the two different materials: fractures in clay are for instance wider than those breaking the cornstarch. It is also worth noting that the proportionality constants inferred from the linear regression we performed on the two sets of experimental data points are of close values (Fig. 3A and 3B).

A new experimental insight is that the characteristic size l of the domains separated by the fractures can be calculated in two different ways: either using expression (4) involving the number of domains N or using (5) that exploits the measured total fracture length L. The use of expression (5) instead of (4) may be more appropriate for FFCs for which the process of identifying and counting domains presents more ambiguities and uncertainties than measuring fracture length.

Finally, it is important to keep in mind that the theory presented in Section 3.3 and hence the power-law relationship between the characteristic domain size and the layer thickness, do not depend on the physical mechanism causing material contraction: the presented results are also valid if shrinking is not caused by drying (Bahr et al., 2010).

5.2. Comparing drying experiments with Lunar FFCs data

In the case where a crater is filled by an exogenous material that subsequently shrinks, the quantity Δd is homologous to the thickness h and a power-law relationship between l_1 or l_2 and Δd

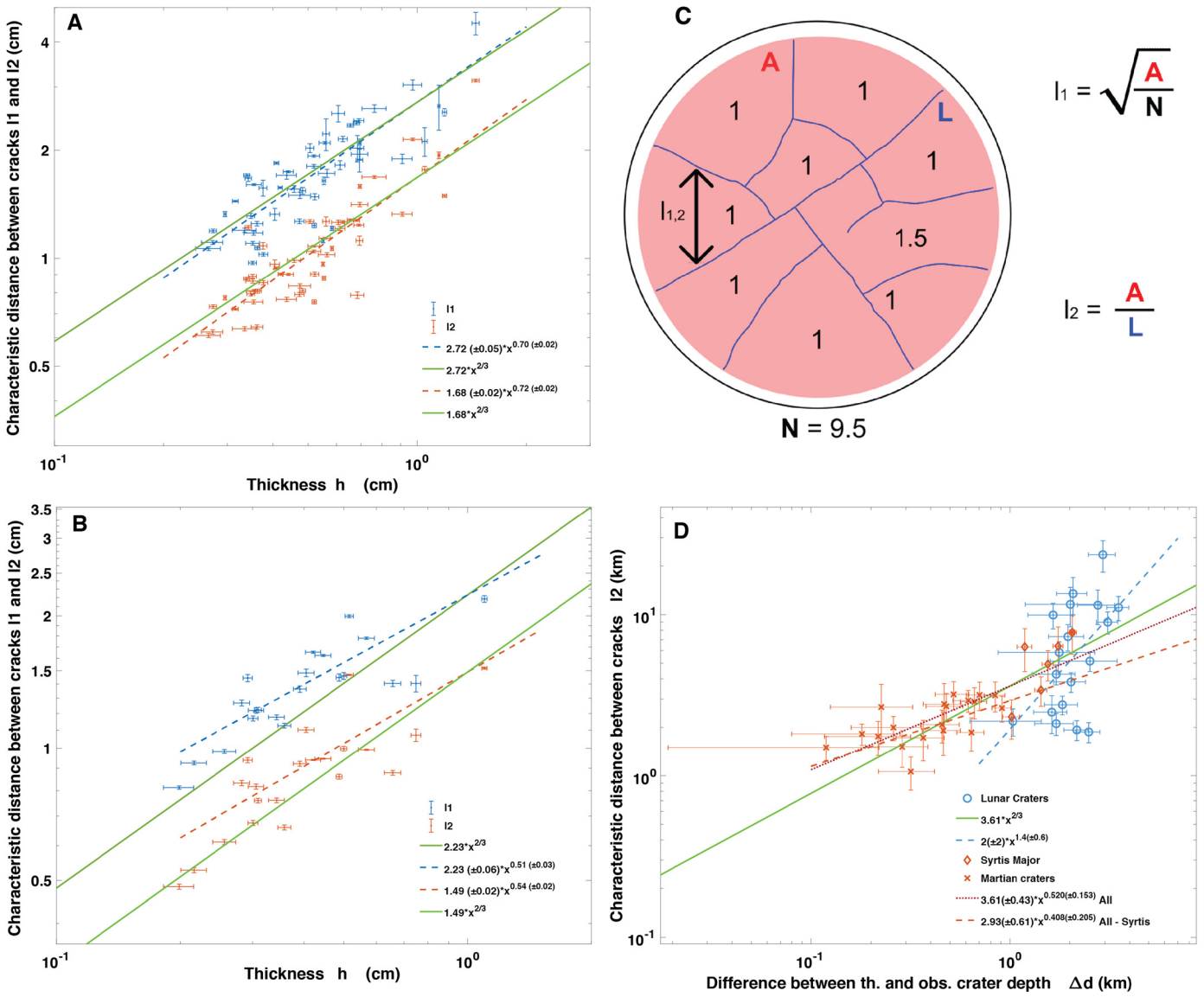

Fig. 3. Characteristic sizes of domains as a function of filling thickness h for experiments in A) cornstarch and B) clay, with l_1 in blue and l_2 in orange symbols for all types of containers. C) Schematic representing the signification of the number of domains N, Area A and characteristic domain size or distance between cracks l_1 and l_2 (Equations (4) and (5)). D) characteristic domain size as a function of Δd for craters on the Moon (blue symbols) and on Mars (orange symbols). The six Martian craters located close to Syrtis Major are represented with a diamond. Best-fit power-law relationships are shown in dashed lines with a colour code that corresponds to the fitted data. The theoretical relationship $l \propto h^{2/3}$ where l is l_1 or l_2 is shown in green.

would be expected. However, hierarchical cracks on the floor of Lunar FFCs are not thought to originate from tensile stresses due to the contraction of material adhering on the crater floor but to result from the emplacement of crater-centred magmatic intrusions (Schultz, 1976; Jozwiak et al., 2012; Thorey and Michaut, 2014; Walwer et al., 2021; Michaut et al., 2020). Indeed, on the contrary to desiccating experiments, lunar FFCs data show no clear relationship between l_1 or l_2 and Δd (Fig. 3C). In addition, while experiments show a general decrease in the number of domains N as the thickness h increases and the container size decreases, such trends are not visible in Lunar FFCs data (Fig. 5). Rather, Lunar FFCs data show a relationship between Δd and the total crack length L that does not exist for experiments (Fig. 4B, Section 4.2) but is appropriate to the uplift and deformation of the roof of an intrusion (see Section 3.2). The crack pattern resulting from the uplift of the crater floor caused by an intrusion probably depends on the intrusion dynamics, its spatial variability and the history of the resulting stress field which, in some cases, may favour a hierarchical crack patterns rather than a more symmetrical pattern such as concentric or radial fractures (Ghabache et al., 2016; Walwer et al., 2021).

5.3. Comparing drying experiments with Martian FFCs

Contrary to Lunar FFCs, our selection of Martian FFCs with a hierarchical crack patterns presents a relationship between the characteristic domain size l_1 or l_2 (given by (4) and (5)) and Δd (Fig. 3D). As for experiments, the number of domains N separated by cracks tends to increase with decreasing values of Δd and increasing values of the crater radius R (Fig. 5). A possible interpretation is that the quantity Δd, for these selected Martian FFCs, corresponds to a thickness of material filling the craters and is, as such, homologous to our definition of h.

Under this assumption, we can verify that the filling thickness Δd of Martian FFCs does not approach the limit where, theoretically, no fractures may be observed because the bulk energy associated to deformation is not large enough. Extrapolating from the power-law relationships obtained for Martian craters on Fig. 3D,

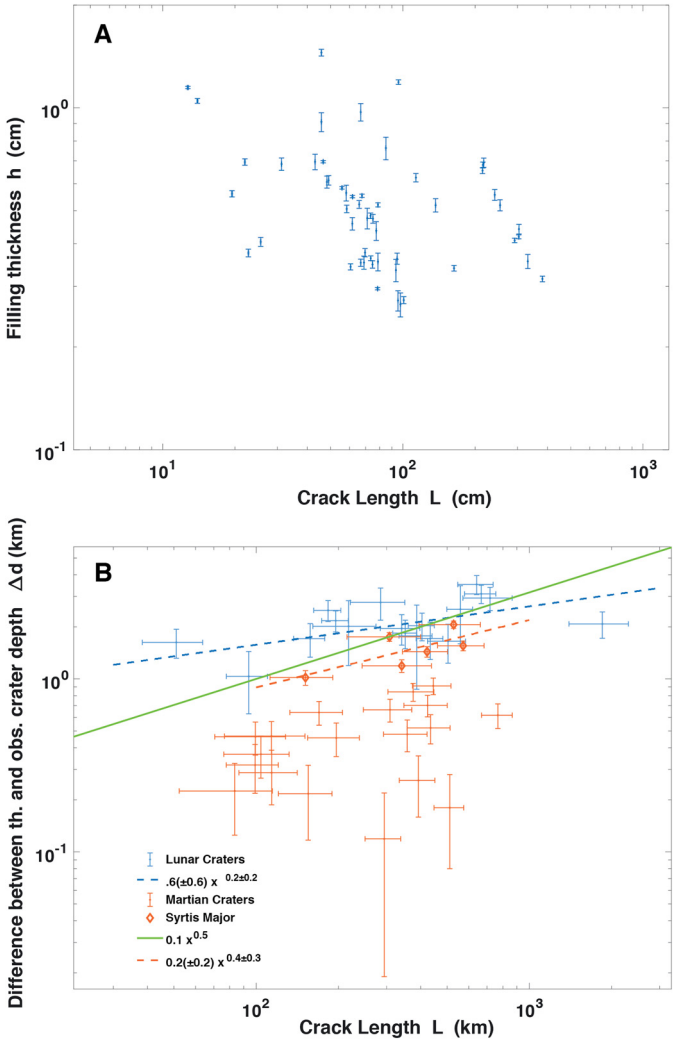

Fig. 4. A) Thickness h as a function of total fracture length L for experiments in cornstarch. B) Difference between theoretical and observed rim-to-floor depth Δd versus fracture length L for FFCs with hierarchical cracks on the Moon (blue) and Mars (orange). The six Martian craters located close to Syrtis Major (within the longitude range $45 - 120^{o}$ E) are represented by diamonds. The best fit power-law relationship between Δd and total crack length is shown in dashed blue line for the Moon and in dashed orange line for the six Martian FFCs located close to Syrtis Major. The theoretical trend $\Delta d \propto \sqrt{L}$ obtained by Walwer et al. (2021) is shown in green.

it is apparent that the characteristic domain size reaches a few tens of kilometres (a typical value for crater diameter) for filling thicknesses larger than ~ 10 km. Given that initial craters depths are only of a few kilometres, this value is clearly too large to be reached.

At least two distinct groups may be identified among our selected craters. First, six Martian craters show Δd and crack characteristics (domain size and total fracture length) that plot among those of Lunar FFCs (Figs. 3C and 4B); they also show a particularly large value of $\Delta d \geq 1$ km. These craters are the six FFCs located close to Syrtis Major (Fig. 2). Taken together, they show a total fracture length that increases with the thickness following a power-law relationship with an exponent equal to 0.39 ± 0.27, similarly to Lunar FFCs (Walwer et al., 2021). The topography of their floors generally appears more chaotic and asymmetric, this latter characteristic may be shared with Lunar FFCs (Jozwiak et al., 2012), compared to that of craters located close to Valles Marineris that appear flatter (see the difference between the more chaotic crater floors on Figures S3 and S4 and the rather flat crater floors on Figures S1 and S2). For these craters, fractures are sometimes associated to large topographic variations that are readily visible on the topographic profiles (see red arrows on Figures S3 and S4). A last observation is that for those six craters, the crater centre is mostly devoid of fractures which are mainly located at its periphery while, for the 19 other craters located close to Valles Marineris, the fractures tend to cross the full crater floor (Figures S1 and S2). Altogether, those observations suggest that those peculiar 6 Martian craters have undergone modifications similar to Lunar FFCs: a crater-centred intrusion potentially caused the observed floor deformation and fracturing at these 6 FFCs located around Syrtis Major.

The 19 craters from the Valles Marineris area show fracture characteristics that present similarities with those generated by desiccation of a hydrated material as their characteristic domain size clearly increases with the filling thickness (Fig. 3B). The key physical ingredients for such a scenario is the filling of the crater by a material adhering on the crater floor, followed by its shrinking by volume loss occurring homogeneously over the entire thickness of material. Hierarchical cracks produced in cornstarch or clay mixed with water indeed affect the whole layer thickness: they do not progress downward but horizontally, reflecting homogeneous volume loss over the material thickness, which explains the homogeneous stress released over the material thickness and hence the hierarchy in between fractures. In the case of drying experiments, capillary flow maintains the water concentration homogeneous over the thin thickness of the desiccating layer (Ma et al., 2019).

5.4. Possible causes of material contraction on the floor of Martian FFCs

Several possible causes have been proposed to explain the formation of fractures on the floor of Martians FFCs that could lead to material contraction inducing tensile stresses.

While density-driven free convection and regional tectonics have been proposed for the origin of large-scale (> 1 km) polygons (Bamberg et al., 2014; Lane and Christensen, 2000), these two scenarios are discarded here since we focus (i) on hierarchical crack patterns, hence cracks presenting T-junction and not Y-junctions that could be characteristic of convection, and (ii) on deformations constrained to the crater interior (we discarded craters with fractures extending beyond the rim, which could be characteristic of regional tectonics).

Loss of water (liquid or solid) from a hydrated mixture deposited within the crater cavity during a flooding event could be a possible mechanism of filling and contraction leading to tensile stresses and fractures (Bamberg et al., 2014; Sato et al., 2010). Martian FFCs located within chaotic terrains, where morphological clues of abundant flows, potentially due to liquid water, could have been subjected to such events (Fig. 2). This region may have experienced a catastrophic water migration event marked by outflow channels which may have filled the craters with hydrated material that subsequently dried (Montgomery and Gillespie, 2005; Andrews-Hanna and Phillips, 2007; Zegers et al., 2010).

However, by analogy with desiccating experiments, one must explain the homogeneous loss of water over a thickness of hundreds of meters (the thickness of the desiccating layer) for this mechanism to produce hierarchical cracks. For desiccating cracks, capillary forces are thought to maintain a vertically homogeneous water content. Large desiccating polygons are observed on Earth, with characteristic sizes reaching up to 300 m (El Maarry et al., 2012). Such giant drying polygons may preferentially be explained by the lowering of the water-table rather than by evaporation (El Maarry et al., 2012). The characteristic domain size of Martian FFCs reaches a few kilometres (Fig. 3) and are thus about one order of magnitude larger than giant polygons on Earth. The character-

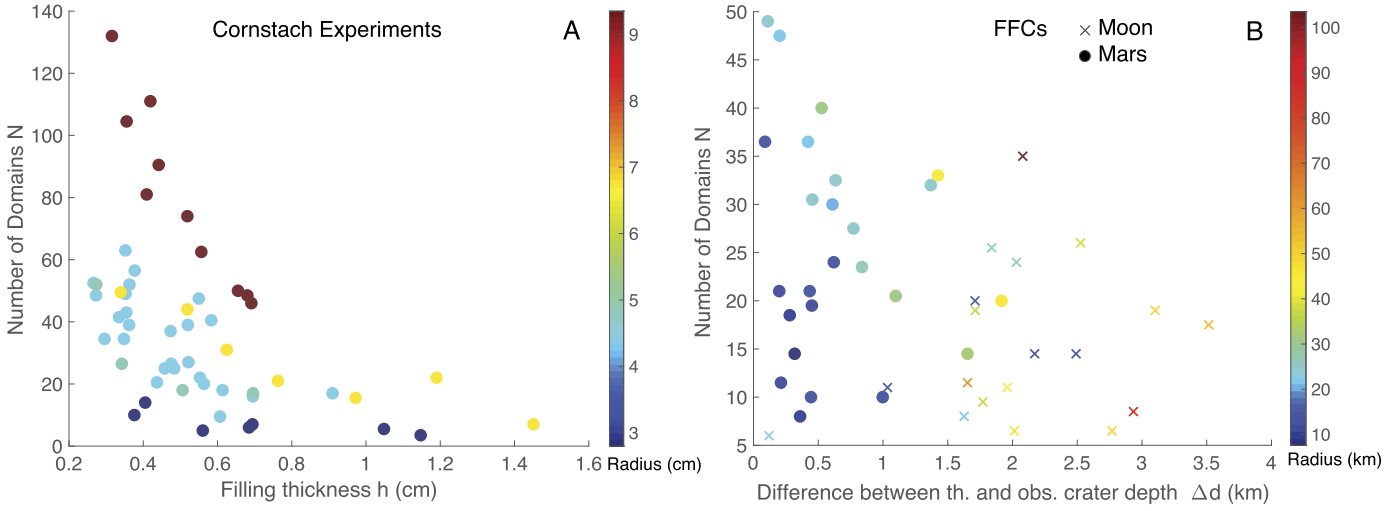

Fig. 5. A) Number of domains N separated by cracks for Cornstach experiments as a function of the thickness h. The colour scale represents the radius of the container. B) Number of domains N separated by cracks on the floor of Martian FFCs (circles) and Lunar FFCs (crosses) as a function of the difference between theoretical and observed crater depth Δd. The colour scale represents the crater radius in kilometre.

istic capillary distance can be ∼3 times larger on Mars than on Earth because of the lower gravity which could partially explain this difference in size. Other topographic observations support the groundwater migration assumption for craters situated East of Valles Marineris. For instance, for FFCs where deformations are not constrained to the crater interior, fractures may extend deeper than the original cavity depth (Sato et al., 2010). For Δd above 1 km however, such as those observed at FFCs located around Syrtis Major, such a process does not seem realistic, in agreement with our interpretation that they probably result from a different process, potentially a magma intrusion as for Lunar FFCs.

Other processes explaining the homogeneous shrinkage of a material adhering the crater floor may involve sublimation of carbonated or water ice. Providing a small crack reaches the base of an ice and sediment mixture, sublimation can then occur over the entire mixture thickness through the fracture itself, triggering its horizontal progression and the formation of new fractures. Heating by an underlying magma intrusion of a mixture of ice and sediments filling the crater floor has also been proposed (Bamberg et al., 2014). Although not the most parsimonious explanation, it cannot really be discarded by this study. Contraction of lava by cooling and solidification does not affect the whole lava thickness homogeneously and progresses from the surface downwards; it thus does not appear as a good candidate to explain the formation of these cracks.

5.5. Limits resulting from FFCs observations

While we believe that the approach here opens interesting perspective to study FFCs on various planetary bodies, we would like to highlight some limitations associated to both observations on FFCs and the assumptions we made. First, the energy necessary to produce the observed fractures depends on the new surfaces created during breaking. As such, it depends on both the observed total fracture length and the unobserved fracture depth. Here, we assumed that the fracture depth is equal to the thickness of the elastic material being deformed (Sections 3.2 and 3.3). In the case where fractures result from contraction of material adhering on a substrate, this choice can be supported by the analogy we made with the drying experiments for which the fractures indeed affect the full material thickness. Assuming that fractures are related to the deformation induced by a magmatic intrusion, this choice is motivated by Lunar FFCs observations showing in some instances vents and extrusive material located onto the fractures suggesting that they extend down to the intrusion depth (Gaddis et al., 2003). Recent experimental set ups aiming at providing analog models of intrusion emplacement in fractured medium (Luzzi et al., 2021; Poppe et al., 2019) also show that fractures may extend from the modelled intrusion depth to the surface. In any case, it is fair to assume that on average the intrusion thickness follows $H = \beta T$ with $0 < \beta \leq 1$, so the relationship between Δd and L displayed in Fig. 4 is modified by a factor $\sqrt{\beta}$.

Another important limit concerns the value Δd calculated from (1) that provides estimations of either crater filling thickness or crater floor uplift. Since the calculation of Δd is based on empirically inferred relationships linking the depth and diameter of fresh craters (Equations (2) and (3)), it is worth questioning whether this relation does not affect the robustness of the observed trend between Δd and either the domain size l or the total fracture length L. The larger the radius, the deeper the crater and the larger the total crack length and floor surface tend to be, which are all quantities that affect the characteristic domain size to filling thickness relationship. In particular, we observe that, for our full set of Martian craters, the crater radius tends to increase with the square root of the filling thickness h or difference between theoretical and observed depth Δd ($R \propto \Delta d^{1/2}$, Fig. 6). Since the crater floor area increases with the square of the crater radius R (and the total crack length tends to increase linearly with R), the characteristic domain size (4), (5) tends to increase linearly with the crater radius (assuming a constant number of domains N). This indirectly imposes a characteristic domain size that varies with the square root of Δd or filling thickness h, as observed. However, eliminating the 6 craters that show the largest values of $\Delta d > 1$ km and that are concordant with Lunar data on Figs. 4B and 3C from our selection of Martian craters removes the radius R to depth difference Δd relationship (Fig. 6). For those 19 craters, the correlation between the domain size and the filling thickness is however still evident (Fig. 3D), confirming the robustness of the trend. The power-law coefficient, equal to 0.4 ±0.2, becomes however smaller than 0.5 (Fig. 3D, see the scaling law in dashed orange line for all Martian craters except those in Syrtis).

6. Conclusion

Crack morphology and quantitative characteristics can be used to constrain the conditions of their formation. Among 155 craters

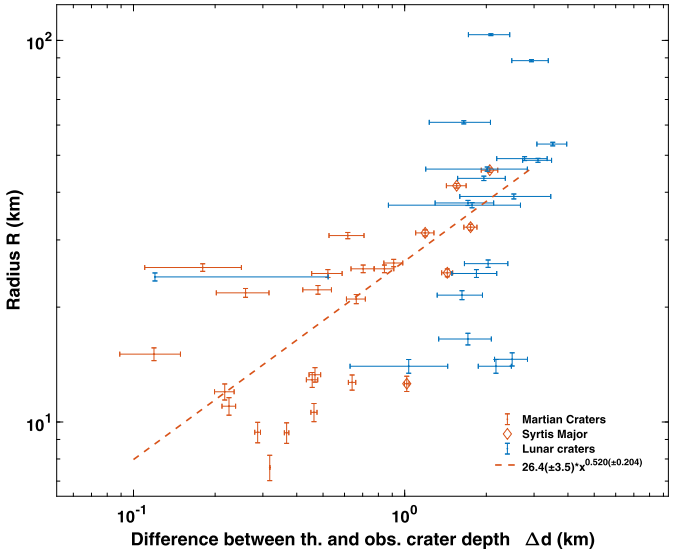

Fig. 6. Radius as a function of the difference between theoretical and observed rim-to-floor depth Δd of FFCs showing hierarchical cracks on the Moon (blue symbols) and on Mars (orange symbols). The six Martian craters located close to Syrtis Major (within the longitude range $45-120^{o}$E) are represented with a diamond.

considered as fractured on the Moon and 383 on Mars, we recognized 19 Lunar and 25 Martian FFCs presenting a well-developed hierarchical fracture patterns constrained to the crater interior. The comparison between this set of craters with laboratory experiments displaying the same pattern suggests that at least two different processes can generate hierarchical cracks on crater floors. One mechanism involves the deformation, uplift and fracturing of an elastic layer overlying a crater-centred intrusion. While such a mechanism can cause radial and concentric fracture patterns, it may also be responsible for the development of hierarchical fracture pattern of Lunar FFCs (Walwer et al., 2021) as well as six Martian craters located around Syrtis Major and the Isidis Basin. A second process involves tensile stresses caused by the shrinking of a material filling the crater and adhering on its floor; it may explain the fracture characteristics observed at 19 other Martian FFCs located East of Valles Marineris. The geological phenomenon at the origin of contraction may involve the loss of water or ice from a sedimentary flow, potentially due to the lowering a water-table, although the size of the domains delimited by cracks is an order of magnitude larger than the largest ones on Earth. Overall, crack qualitative and quantitative characteristics used together with scaling laws derived from Griffith's theory appear as interesting tools to constrain processes leading to FFCs formation.

CRediT authorship contribution statement

Axel Montigny: Formal analysis, Investigation, Validation, Visualization, Writing – original draft. **Damian Walwer:** Conceptualization, Formal analysis, Investigation, Validation, Visualization, Writing – review & editing. **Chloé Michaut:** Conceptualization, Funding acquisition, Methodology, Project administration, Resources, Supervision, Validation, Visualization, Writing – review & editing.

Declaration of competing interest

The authors declare that they have no known competing financial interests or personal relationships that could have appeared to influence the work reported in this paper.

Data availability

Data are provided as supplementary material (several tables in .txt files)

Acknowledgements

We thank two anonymous reviewers for their helpful comments on our manuscript. Emmanuelle Albalat and Florent Arnaud-Godet are thanked for their help in the lab. DW is sincerely grateful to Mokhtar Adda-Bedia for stimulating discussions about fracture physics in general and fracture patterns in particular that originated some of the ideas presented in this study. This project has been supported by the Institut Universitaire de France and has received funding from the European Research Council (ERC) under the European Union Horizon 2020 research and innovation programme (grant agreement No. 101001689). DW acknowledges support from the College of Earth and Mineral Sciences of Pennsylvania State University as well as NSF Geophysics grants EAR 1923943 and EAR 2151005.

Appendix A. Supplementary material

Supplementary material related to this article can be found online at https://doi.org/10.1016/j.epsl.2022.117887.

References

Allain, C., Limat, L., 1995. Regular patterns of cracks formed by directional drying of a colloidal suspension. Phys. Rev. Lett. 74, 2981–2985.
Andrews-Hanna, J.C., Phillips, R.J., 2007. Hydrological modeling of outflow channels and chaos regions on Mars. J. Geophys. Res., Planets 112. https://doi.org/10.1029/2006je002881.
Bahr, H.-A., Weiss, H.-J., Bahr, U., Hofmann, M., Fischer, G., Lampenscherf, S., Balke, H., 2010. Scaling behavior of thermal shock crack patterns and tunneling cracks driven by cooling or drying. J. Mech. Phys. Solids 58 (9), 1411–1421.
Bamberg, M., Jaumann, R., Asche, H., Kneissl, T., Michael, G.G., 2014. Floor-fractured craters on Mars, observations and origin. Planet. Space Sci. 98 (C), 142–162.
Bohn, S., Pauchard, L., Couder, Y., 2014a. Hierarchical crack pattern as formed by successive domain divisions. I. Temporal and geometrical hierarchy. Phys. Rev. E 71. https://doi.org/10.1103/PhysRevE.71.046214.
Bohn, S., Platkiewicz, J., Andreotti, B., Adda-Bedia, M., Couder, Y., 2014b. Hierarchical crack pattern as formed by successive domain divisions. II. From disordered to deterministic behaviour. Phys. Rev. E 71. https://doi.org/10.1103/PhysRevE.71.046215.
Boyce, J.M., Garbeil, H., 2007. Geometric relationships of pristine martian complex impact craters, and their implications to Mars geologic history. Geophys. Res. Lett. 34. https://doi.org/10.1029/2007GL029731.
Buczkowski, D.L., Sizemore, H.G., Bland, M.T., Scully, J.E.C., Quick, L.C., Hughson, K.H.G., Park, R.S., Preusker, F., Raymond, C.A., Russell, C.T., 2018. Floor-fractured craters on Ceres and implications for interior processes. J. Geophys. Res., Planets 123, 3188–3204.
Cho, H.J., Datta, S.S., 2019. Scaling law for cracking in shrinkable granular packings. Phys. Rev. Lett. 123. https://doi.org/10.1103/PhysRevLett.123.158004.
Cohen, Y., Mathiesen, J., Procaccia, I., 2009. Drying patterns: sensitivity to residual stresses. Phys. Rev. E 79 (4), 046109.
Dufresne, E.R., Corwin, E.I., Greenblatt, N.A., Ashmore, J., Wang, D.Y., Dinsmore, A.D., Cheng, J.X., Xie, X.S., Hutchinson, J.W., Weitz, D.A., 2003. Flow and fracture in drying nanoparticle suspensions. Phys. Rev. Lett. 91 (22). https://doi.org/10.1103/PhysRevLett.91.224501.
El Maarry, M.R., Kodikara, J., Wijessoriya, S., Markiewicz, W.J., Thomas, N., 2012. Desiccation mechanism for formation of giant polygons on Earth and intermediate-sized polygons on Mars: results from a pre-fracture model. Earth Planet. Sci. Lett. 323–324, 19–26.
Flores, J.C., 2017. Mean-field crack networks on desiccated films and their applications: Girl with a Pearl Earring. Soft Matter 13, 1352–1356.
Gaddis, L.R., Staid, M.I., Tyburczy, J.A., Hawke, B.R., Petro, N.E., 2003. Compositional analyses of lunar pyroclastic deposits. Icarus 161 (2), 262–280.
Gauthier, G., Lazarus, V., Pauchard, L., 2010. Shrinkage star-shaped cracks: explaining the transition from 90 degrees to 120 degrees. Europhys. Lett. 89 (2), 26002.
Ghabache, E., Josserand, C., Séon, T., 2016. Frozen impacted drop: from fragmentation to hierarchical crack patterns. Phys. Rev. Lett. 117 (7), 074501.
Griffith, A.A., 1921. The phenomena of rupture and flow in solids. Philos. Trans. R. Soc. A, Math. Phys. Eng. Sci. 221 (582–593), 163–198. http://rsta.royalsocietypublishing.org/cgi/doi/10.1098/rsta.1921.0006.

Hall, J.L., Salomon, S.C., Head, J.W., 1981. Lunar floor-fractured craters: evidence for viscous relaxation of crater topography. J. Geophys. Res., Planets 86, 9537–9552.
Head, J.W., Wilson, L., 2017. Generation, ascent and eruption of magma on the Moon: new insights into source depths, magma supply, intrusions and effusive/explosive eruptions (Part 2: predicted emplacement processes and observations). Icarus 283, 176–223.
Jozwiak, L.M., Head, J.W., Zuber, M.T., Smith, D.E., Neumann, G.A., 2012. Lunar floor-fractured craters: classification, distribution, origin and implications for magmatism and shallow crustal structure. J. Geophys. Res., Planets 117. https://doi.org/10.1029/2012JE004134.
Korteniemi, J., Aittola, M., Öhman, T., Raitala, J.T., 2006. Floor-fractured craters on the terrestrial planets - the martian perspective. In: Proceedings of the First International Conference on Impact Cratering in the Solar System, vol. 612, pp. 193–198.
Landau, L.D., Lifshitz, E.M., Kosevich, A.M., Pitaevskii, L.P., 1986. Theory of Elasticity, vol. 7. Elsevier.
Lane, M., Christensen, P.R., 2000. Convection in a catastrophic flood deposit as the mechanism for giant polygons on Mars. J. Geophys. Res. 105, 17617–17627.
Luzzi, E., Rossi, A.P., Massironi, M., Pozzobon, R., Corti, G., Maestrelli, D., 2021. Caldera collapse as the trigger of chaos and fractured craters on the Moon and Mars. Geophys. Res. Lett. 48 (11). https://doi.org/10.1029/2021GL092436.
Ma, X., Lwenson, J., Burton, J.C., 2019. Universal scaling of polygonal desiccation crack patterns. Phys. Rev. E 99. https://doi.org/10.1103/PhysRevE.99.012802.
Michaut, C., 2011. Dynamics of magmatic intrusions in the upper crust: theory and applications to laccoliths on Earth and the Moon. J. Geophys. Res. 116. https://doi.org/10.1029/2010JB008108.
Michaut, C., Pinel, V., 2018. Magma ascent and eruption triggered by cratering on the Moon. Geophys. Res. Lett. 45. https://doi.org/10.1029/2018GL078150.
Michaut, C., Pinel, V., Maccaferri, F., 2020. Magma ascent at floor-fractured craters diagnoses the lithospheric stress state on the Moon. Earth Planet. Sci. Lett. 530. https://doi.org/10.1016/j.epsl.2019.115889.
Montgomery, D.R., Gillespie, A., 2005. Formation of Martian outflow channels by catastrophic dewatering of evaporite deposits. Geology 33 (8). https://doi.org/10.1130/G21270AR.1.
Pike, R.J., 1977. Size-dependence in the shape of fresh impact craters on the Moon. In: Impact and Explosion Cratering. Pergamon Press, New York, pp. 489–509.
Pollard, D., Johnson, A., 1973. Mechanics of growth of some laccolithic intrusions in the Henry Mountains, Utah, II. Bending and failure of overburden layers and sill formation. Tectonophysics 18, 311–354.
Poppe, S., Holohan, E.P., Galland, O., Buls, N., Van Gompel, G., Keelson, B., Tournigand, P.-Y., Brancart, J., Hollis, D., Nila, A., et al., 2019. An inside perspective on magma intrusion: quantifying 3D displacement and strain in laboratory experiments by dynamic X-ray computed tomography. Earth Sci. Front. 7, 62.
Robbins, S.J., Hynek, B.N., 2012. A new global database of Mars impact craters $\geq$ 1 km: 2. Global crater properties and regional variations of the simple-to-complex transition diameter. J. Geophys. Res., Planets 117, E6001. https://doi.org/10.1029/2011JE003966.
Sato, H., Kurita, K., Baratoux, D., 2010. The formation of floor-fractured craters in Xanthe Terra. Icarus 207, 248–264.
Schultz, P.H., 1976. Floor-fractured lunar craters. Moon 15, 241–273.
Schultz, P.H., 1978. Martian intrusions: possible sites and implications. Geophys. Res. Lett. 5 (6), 457–460.
Tang, C., Zhang, Y., Liang, Z., Xu, T., Tham, L., Lindqvist, P.-A., Kou, S., Liu, H., 2006. Fracture spacing in layered materials and pattern transition from parallel to polygonal fractures. Phys. Rev. E 73 (5), 056120.
Thorey, C., Michaut, C., 2014. A model for the dynamics of crater-centered intrusions: application to lunar floor-fractured craters. J. Geophys. Res., Planets 119, 286–312.
Thorey, C., Michaut, C., Wieczorek, M., 2015. Gravitational signatures of lunar floor-fractured craters. Earth Planet. Sci. Lett. 424, 269–279.
Vandenberghe, N., Vermorel, R., Villermaux, E., 2013. Star-shaped crack pattern of broken windows. Phys. Rev. Lett. 110 (17), 174302.
Vermorel, R., Vandenberghe, N., Villermaux, E., 2010. Radial cracks in perforated thin sheets. Phys. Rev. Lett. 104 (17), 175502.
Walwer, D., Michaut, C., Pinel, V., Adda Bedia, M., 2021. Magma ascent and emplacement below floor fractured craters on the Moon from floor uplift and fracture length. Phys. Earth Planet. Inter. 312. https://doi.org/10.1016/j.pepi.2021.106658.
Wichman, R., Schultz, P., 1996. Crater-centered laccoliths on the Moon: modeling intrusion depth and magmatic pressure at the crater Taruntius. Icarus 122 (1), 193–199.
Wichman, R.W., Schultz, P.H., 1995. Floor-fractured craters in Mare Smythii and west of Oceanus Procellarum. Implications of crater modification by viscous relaxation and igneous intrusion models. J. Geophys. Res., Planets 100, 21,209–21,218.
Wilson, L., Head, J.W., 2017. Generation, ascent and eruption of magma on the Moon: new insights into source depths, magma supply, intrusions and effusive/explosive eruptions (Part 1: theory). Icarus 283, 146–175.
Zegers, T.E., Oosthoek, J.H.P., Rossi, A.P., Blom, J.K., Schumacher, S., 2010. Melt and collapse of buried water ice: an alternative hypothesis for the formation of chaotic terrains on Mars. Earth Planet. Sci. Lett. 297, 496–504.